LINEAR CONTROL OF SIDE FORCES AND YAWING MOMENTS USING THE DYNAMIC MANIPULATION OF FOREBODY VORTICES*

R. Lee**
Carleton University, Ottawa, Canada

E.S. Hanff†
National Research Council, Ottawa, Canada

R.J. Kind‡
Carleton University, Ottawa, Canada

Abstract

A technique is proposed in which the behaviour of forebody vortices, arising at high angles of attack, is dynamically manipulated to generate aerodynamic side forces and yawing moments suitable for directional control of a fighter aircraft under conditions where a conventional rudder will lose its effectiveness. The scheme exploits the bi-stable nature of the vortices by forcing them to switch between their stable states at high frequency. Alternating blowing from two forward-facing nozzles located near the apex of the forebody is employed to trigger the vortex switching. A wind-tunnel experiment conducted to determine the potential of the technique showed that at zero sideslip, time-average side force and yawing moment vary linearly with duty cycle, vanishing at 50% duty cycle. The effectiveness of the method was demonstrated at a Reynolds number of 1.76×10^5 with a minimum blowing momentum coefficient of 0.00066 and a maximum reduced frequency of 0.32. In the presence of sideslip, the linear variation of the time-average loads is retained to some extent but their symmetry is about non-zero loads. Unsuitable nozzle location is suspected as the cause for the sensitivity to sideslip and also for the absence of vortex control at higher Reynolds numbers.

Nomenclature

C_n	Yawing moment coefficient, $\frac{N}{q_\infty S l_{ref}}$
$\overline{C}_n$	Time-average yawing moment coefficient
C_y	Side force coefficient, $\frac{Y}{q_\infty S}$
$\overline{C}_y$	Time-average side force coefficient
d	Nozzle diameter
$C\mu$	Coefficient of blowing momentum, $\frac{\dot{m}_j V_j}{q_\infty S}$
D	Base diameter of model
l_{ref}	Overall length of model
$\dot{m}_j$	Nozzle mass flowrate, $\rho \frac{\pi}{4} d^2 V_j$
N	Yawing moment relative to the resolving center of the internal balance
q_∞	Freestream dynamic pressure, $\frac{1}{2}\rho {V_\infty}^2$
Re_D	Reynolds number, $\frac{V_\infty D}{\nu}$
S	Reference area, $\frac{\pi D^2}{4}$
T	Period of an alternating blowing cycle
V_∞	Freestream velocity
V_j	Blowing velocity at nozzle exit
x	Longitudinal location of nozzle exit relative to the nose apex
Y	Side force
α	Angle of attack
β	Angle of sideslip
ν	Kinematic viscosity
ρ	Density
σ	Body-axis inclination to freestream velocity (i.e., the turntable angle)
τ	Duration a valve is open during the alternating blowing cycle
ϕ	Roll angle
ω	Angular frequency of alternating blowing, radians/time
ω^*	Reduced frequency of alternating blowing, $\frac{\omega D}{V_\infty}$

* Work conducted under the Joint Research Program of U.S. Air Force Office for Scientific Research, Flight Dynamics Directorate/Wright Laboratory, the Institute for Aerospace Research of the National Research Council of Canada, and the Canadian Department of National Defence.

**Graduate Student, Dept. of Mechanical and Aerospace Engineering, Carleton University, Ottawa, Canada.
†Senior Research Officer, Aerodynamics Laboratory, National Research Council, Ottawa, Canada, Member AIAA.
‡Professor, Dept. of Mechanical and Aerospace Engineering, Carleton University, Ottawa, Canada, Associate Fellow AIAA.

Introduction

The conventional belief that tactical air superiority will be achieved by fighter aircraft engaging adversaries at beyond-visual-range with long-range missiles, would seem to be destined for obsolescence in the face of the emerging confidence in low-observables technology and electronic warfare countermeasures. These technologies hamper a pilot's ability to confidently identify an adversary at beyond-visual range. This difficulty, coupled with the uncertain success of a long-range missile, forces a pilot into short-range combat tactics with the possibility of engaging a superior number of adversaries. In this situation, agility and maneuverability of a fighter aircraft are essential to achieve tactical effectiveness and enhance combat survivability. Simulation studies have shown that near- and post-stall maneuverability and agility – the ability to perform rapid and controlled maneuvers at high angles of attack – are a necessary component to achieve these objectives. Flight tests of experimental aircraft equipped with thrust vectoring capabilities, such as the X-31, F-18 HARV and F-16 MATV, have confirmed the simulation findings.[1]

Another attractive approach for augmenting directional controllability at high angle of attack, is the manipulation of forebody vortices which permits the generation of significant aerodynamic side forces and yawing moments after a conventional rudder has lost its effectiveness. Forebody vortex manipulation has been the focus of extensive research activity for several years. The manipulation methods currently under investigation are essentially steady schemes.[2] That is, quasi-steady loads are generated by forcing the forebody vortices to assume prescribed positions with respect to the forebody so that desired control forces or moments are generated. Inasmuch as forebody vortex positions are inherently bi-stable (see Figure 1) over a significant range of angles of attack, the steady methods involve first forcing the vortices to adopt a symmetrical arrangement, typically by tailoring the forebody geometry, and then altering their position by pneumatic or mechanical means to generate the desired control forces or moments. The need to overcome the artificially induced symmetry may require considerable power and, furthermore, it is difficult to implement control laws due to the often severely non-linear behaviour of the resulting loads.

A novel dynamic vortex manipulation scheme has recently been proposed which has the potential of avoiding the above two problems. It exploits the bi-stable nature of the vortex pattern and makes use of the fact that minute disturbances in the flow at the nose can cause switching between the two stable states.[3] Specifically, the forebody vortex pattern is deliberately switched back and forth between its two stable states at a frequency sufficiently high that the aircraft cannot respond significantly to the resulting instantaneous loads because of its inertia. The aircraft would, however, respond to the time-average loads generated by the vortex manipulation. These loads can be controlled by varying the fraction of the switching-cycle period during which the vortex pattern is in one or the other state, i.e., by modulating the switching duty cycle. The concept is illustrated in Figure 2(a) and the expected effect of changing the duty cycle is shown in Figure 2(b). The perturbation required at the apex of the forebody can be introduced by pneumatic or mechanical means.

Preliminary water-tunnel experiments using alternating forward blowing showed that very low blowing coefficients were required to reliably switch the forebody vortices from one stable configuration to the other and that switching at a reasonably high reduced frequency was possible.[3] Only a duty cycle of 50% ($\tau/T = 0.5$) was investigated and the maximum Reynolds number was only about 7000.

This paper describes a follow-on wind-tunnel investigation of the dynamic manipulation concept. The work had two main objectives: to determine the variation of time-average side force over a blowing duty cycle range of 0 to 100% for various reduced frequencies, and to investigate performance at higher Reynolds numbers. To ensure consistency with the water tunnel investigation, forward blowing was retained as the chosen vortex manipulation method and the model shape as well as nozzle location were essentially unchanged. In addition to measuring side force and yawing moment, surface oil and laser-sheet flow visualization tests were conducted. The experiments confirmed the potential of the dynamic manipulation approach. In particular, switching of the vortices was possible with even lower blowing momentum and at higher reduced frequency than reported by Alexan *et al.*[3]

Experimental Setup

The investigation was performed in the 2m × 3m low-speed wind tunnel at the Institute for Aerospace Research (IAR). A tangent ogive-cylinder model was sting-mounted on a symmetric strut that spanned the test section to avoid asymmetric support interference (Figure 3). Angle of attack was adjusted by

synchronously rotating the floor and roof turntables that supported the strut, while sideslip was obtained by rolling the model about its axis. Blockage effects due to the model were considered to be insignificant as its projected area at $\alpha = 90°$ was only about 2% of the test section cross-sectional area.

A schematic of the model is shown in Figure 4. The ogive nose had a radius of 715.2mm and a 56° included angle at the apex. It was fitted with two forward-blowing nozzles, aligned parallel to the longitudinal axis and located as shown in Figure 4. The nozzles had an internal diameter of 2.44mm and the exits were located 34mm from the apex of the nose (i.e., d/D = 0.018 and x/D = 0.25). Each nozzle was fed with pressurized air through a high speed, solenoid-actuated on-off valve located inside the nose, approximately 30cm aft of the nozzle exits. Air supply pressure was controlled by a regulator outside the wind tunnel and monitored by a piezoresistive pressure transducer. The nozzle flow rates were calibrated in terms of the pressure upstream of restrictors located between the valves and corresponding nozzle exits. Side forces and yawing moment were measured in the body-axis frame of reference with an internal two-component strain gauge balance. The balance measured yawing moments to within ±2.5% of the largest observed value and was virtually insensitive to normal loads.

The data acquisition system, a customized PC-based real-time system with a maximum throughput of 20 kHz, was used to monitor the strain gauge bridges and pressure transducers. The system also generated the signals for the two soleniod valves, providing control of the frequency and duty cycle. The signals from the pressure transducers and strain gauges were ensemble-averaged over a substantial number of cycles. In each run, the operator allowed the averaging process to continue until the ensemble-averages had stabilized.

To visualize the flow, a laser light sheet normal to the model axis was used to illuminate the smoke-seeded flow. The sheet could be moved to any axial station by means of a traversing mechanism. Images were recorded by means of an image-intensified high-speed video camera operating at 250 frames/second, located outside the test section in front of the model. A diode laser beam, synchronous with the port valve, illuminated a spot on the model to provide a valve-state indicator on each video image. Surface flow visualization was performed with a mixture of oil and a pigment that fluoresced under ultraviolet light. A high-resolution video camera was used to record the evolution of the surface patterns.

Most of the experimental data was obtained at a wind speed of 19 m/s (63 ft/s), which corresponds to a Reynolds number $Re_D = 1.76 \times 10^5$. Some tests were performed at $V_\infty = 38$ m/s (125 ft/s) and 70 m/s (230 ft/s), corresponding to $Re_D = 3.53 \times 10^5$ and 6.50×10^5 respectively. The model was inclined to the freestream (σ) from 30° to 70° in 10° increments. For non-zero sideslip tests, the roll angle of the sting was set to ±5°, ±10°, ±15° and ±20°.

Results and Discussion

The axis system and sign conventions are defined in Figure 4. Side force, Y, is positive to starboard and produces a positive yawing moment when applied forward of the resolving center of the balance, located approximately 46.5 cm aft of the nose apex. The sideslip angle, β, is considered positive when the model is yawed to port. Coefficients of blowing momentum ($C\mu$), side force (C_y), and yawing moment (C_n) are based on freestream dynamic pressure, base area and model length. Values for $\overline{C}_y$ and $\overline{C}_n$ were obtained by time-averaging C_y and C_n over one blowing cycle.

Minimum Blowing Coefficient

Under high angle of attack conditions with steady blowing from one nozzle, C_y and C_n increase sharply as $C\mu$ is increased from zero until a plateau is reached, beyond which further increases in $C\mu$ produce little change in these loads. The value of $C\mu$ required to reach the plateau is referred to as the minimum blowing coefficient. The effect of $C\mu$ on C_y was investigated for steady blowing at angles of attack of 40°, 50° and 60°. The results for $Re_D = 1.76 \times 10^5$, presented in Figure 5, show that the side force response to steady port and starboard blowing is nearly symmetric about the origin, and at all angles of attack the side force reaches a plateau for $C\mu$ near 0.00050. For $\alpha = 50°$, $C\mu = 0.00066$ was regarded as the minimum blowing coefficient. For this value, the blowing effectiveness, $C_y/C\mu$, is more than 5500. These results represent an improvement over Alexan's water-tunnel findings by a factor of 2 for the minimum blowing coefficient, and about 2.75 for the blowing effectiveness.[4] Investigation at $Re_D = 2.82 \times 10^5$ found the minimum blowing coefficient to be approximately 0.00053.

Steady Blowing, Zero Sideslip

Figure 6 shows the side force and yawing moment response to steady blowing through a sin-

gle port with $C\mu = 0.00066$, for zero sideslip at $Re_D = 1.76 \times 10^5$. The baseline curve illustrates the response without blowing. The presence of an asymmetry in the forebody vortex pattern is clearly manifested by significant non-zero side forces for $\alpha > 40°$. At this Reynolds number the pattern is reliably controlled by blowing; that is, starboard blowing always gives negative side force and vice versa. The side force starts increasing at $\alpha = 30°$, reaching a maximum at $\alpha = 50°$, then decreases towards $\alpha = 70°$. An important feature of the results with blowing is that the port and starboard responses are nearly symmetrical.

At higher Reynolds numbers, the baseline and steady blowing behaviour are markedly different from those at the lower Re_D. Specifically, the steady blowing responses do not have the symmetrical characteristic previously observed. Of particular concern are the blowing responses at $Re_D = 6.50 \times 10^5$, shown in Figure 7. At this Reynolds number, a rather modest side force could be obtained but it was insufficient to overcome the baseline asymmetry, a situation that did not improve by increasing the blowing coefficient to 0.00094 from a minimum of 0.00066. The reasons for this behaviour are not clear at this time, but it seems that improper nozzle location could be important. As mentioned earlier, the nozzles were at the same location as those used in the previous water-tunnel tests, where the small size of the model made it impractical to place them closer to the tip. Further tests are planned in which the nozzles will be located further forward with the expectation that such a position will render the blowing more effective in influencing the three-dimensional separation at high Reynolds numbers. In view of the disappointing results at the higher Reynolds numbers investigated, the bulk of the dynamic manipulation tests were performed at $Re_D = 1.76 \times 10^5$ where excellent blowing effectiveness was observed.

Alternating Blowing, Zero Sideslip

Alternating blowing causes the side force to change orientation as the forebody vortex pattern oscillates between the two stable states. If the switching frequency is sufficiently low, the vortex pattern should be able to follow the alternating blowing. That is, quasi-steady behaviour is expected and the time-average side force is expected to vary linearly with the duty cycle parameter τ/T, as illustrated in Figure 2. At higher frequencies, aerodynamic lag effects become significant and the short time available does not allow the side forces to develop fully at low τ/T. That is, quasi-steady behaviour no longer prevails and a non-linear variation with duty cycle is expected to occur in that region. The frequency at which a non-linearity appears for τ/T over a prescribed range (e.g., $0-0.1$ or $0.9-1.0$) is regarded to be the "maximum reduced frequency".

Figure 8 and Figure 9 show the variation of side force and yawing moment with duty cycle parameter, τ/T, for alternating blowing reduced frequencies $\omega^* = 0.16$ (3.6 Hz) and 0.32 (7.2 Hz) respectively, at $C\mu = 0.00066$ and $Re_D = 1.76 \times 10^5$. Note that at $\tau/T = 0$ the port valve is closed and the starboard valve is fully open throughout the blowing cycle; for $\tau/T = 1$, the state of the valves is the opposite. Clearly the side force and yawing moment vary linearly with duty cycle and vanish at $\tau/T = 0.5$, which is consistent with the behaviour illustrated in Figure 2. At $\alpha = 30°$, 40° and 50° the linearity of $\overline{C}_y$ and $\overline{C}_n$ is very good throughout the range of τ/T for both $\omega^* = 0.16$ and 0.32. A slight non-linearity is observed in $\overline{C}_y$ and $\overline{C}_n$ for $\omega^* = 0.16$ at $\alpha = 60°$; but for $\omega^* = 0.32$, the non-linearity at $\alpha = 60°$ is much more obvious. Consequently, $\omega^* = 0.32$ was considered to be the maximum reduced alternating frequency, corresponding to twice the value found in the water-tunnel experiments (at $Re_D \approx 7000$). Smoke flow visualization tests showed that the vortices respond well at this alternating blowing frequency over the range of duty cycle.

Alternating Blowing, Non-zero Sideslip

Figure 10 shows that at non-zero sideslip ($\phi = 10°$) the load linearity seen in Figure 9 is retained to a substantial extent but the symmetry of the various curves is now about finite values of the loads and depends to some extent on angle of attack. This effect becomes more important at larger sideslip angles. The effect of sideslip on $\overline{C}_y$ is illustrated in Figure 11. The results presented are for steady blowing with $C\mu = 0.00066$ at $\sigma = 50°$ and $Re_D = 1.76 \times 10^5$. For $\phi < 0°$ (negative sideslip), positive $\overline{C}_y$ increases while negative $\overline{C}_y$ diminishes in magnitude; for $\phi > 0°$ (positive sideslip), the effect is the opposite. Surface visualization observations show that in negative sideslip, for example, the port nozzle is closer to the port primary separation line thereby improving the influence of the efflux on the port vortex. By contrast, the starboard nozzle is farther away from its corresponding primary separation line. This sensitivity to sideslip would seem to be an effect of nozzle location and/or nose bluntness since Roos and Magness found little sensitivity to sideslip over a comparable range of sideslip.[5]

Conclusions

This investigation has confirmed the potential of dynamic forebody vortex manipulation as a means of obtaining directional control at high angles of attack. It has shown that time-average side force and yawing moment can be made to vary linearly with blowing duty cycle, making the method attractive from a controls point of view. Although the behaviour of time-average loads was excellent at zero sideslip, it showed some undesirable features at non-zero sideslip angles.

The controlled manipulation of forebody vortices was found to be possible with a minimum blowing momentum coefficient of 0.00066 at $Re_D = 1.76 \times 10^5$, giving a ratio $C_y/C\mu$ of more than 5500. The maximum reduced frequency of alternating blowing for effective control was found to be 0.32, which is approximately twice that observed in the previous water-tunnel experiments.

Performance at Reynolds numbers above 1.8×10^5 was disappointing due to poor response of the forebody vortices to the blowing. Unsuitable nozzle location is thought to be responsible for this as well as for the undesirable behaviour with sideslip. It is expected that locating the nozzles closer to the tip will correct these problems.

Future Work

The research on the dynamic manipulation of forebody vortices is continuing. An experimental program has been planned to elucidate the issues of Reynolds number dependency and effects of sideslip. Three objectives have been established for this program: (1) to establish the physical reasons for the apparent Reynolds number effect on the effectiveness of the technique; (2) to optimize the location of forward-blowing nozzles and develop an understanding of the factors which determine the optimum location; and (3) if possible, to demonstrate that the technique can provide reliable directional control of a partially constrained aircraft model.

Unlike the previous investigation, a full aircraft configuration (i.e., fuselage, wing, and vertical tail) will be used in this series of wind-tunnel tests (Figure 12). The generic fighter aircraft model has a 65° delta wing and a long, ogive forebody with a circular cross-section. The forebody has an apex semi-angle of 12.8° and accomodates a pneumatic forward-blowing system similiar to the one described earlier. In particular, the tip of the forebody has been designed to be removable, allowing different nozzle configurations to be tested.

Testing will be conducted in the IAR $2m \times 3m$ low-speed wind tunnel with the model stationary. Force and moment measurements will be used to find the optimum nozzle location and off-surface flow visualization will be employed to observe the motion of the forebody vortices. Surface flow visualization will be used to investigate the interaction between the nozzle flux and forebody vortices. If stationary test results prove to be positive, the effectiveness of the forebody vortex manipulation method will be assessed in experiments in which forebody blowing will be used to control the motion of the model in a free-to-roll (about the velocity vector) setup.

Acknowledgments

The authors wish to acknowledge the contribution of A. Prini in developing and operating the data acquisition system and that of H. Xia in recording the flow visualization tests.

References

[1] Flynn, B., Smith, R.E., and Schnider, E., "Thrust Vectoring: A New Dimension", *Canadian Aeronautics and Space Journal*, Volume 41, No. 4, December 1995, pp. 171-178.

[2] Malcolm, G., "Forebody Vortex Control - A Progress Review", AIAA Paper No. 93-3540-CP, August 1993.

[3] Alexan, K., Hanff, E.S., and Kind, R.J., "Water-Tunnel Investigation of Dynamic Manipulation of Forebody Vortices", AIAA Paper No. 94-0503, January 1994.

[4] Lee, R., "A Wind-tunnel Investigation of the Dynamic Manipulation of Forebody Vortices", M. Eng. Thesis, Dept. of Mechanical and Aerospace Engineering, Carleton University, Ottawa, Canada, April 1995.

[5] Roos, F.W., and Magness, C.L., "Bluntness and Blowing for Flowfield Asymmetry Control on Slender Forebodies", AIAA Paper No. 93-3409, August 1993.

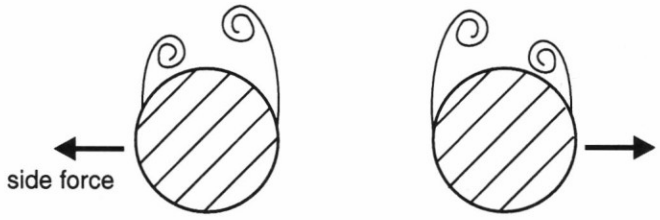

Figure 1 – Two stable vortex patterns in a cross-flow plane on a forebody at a high angle of attack.

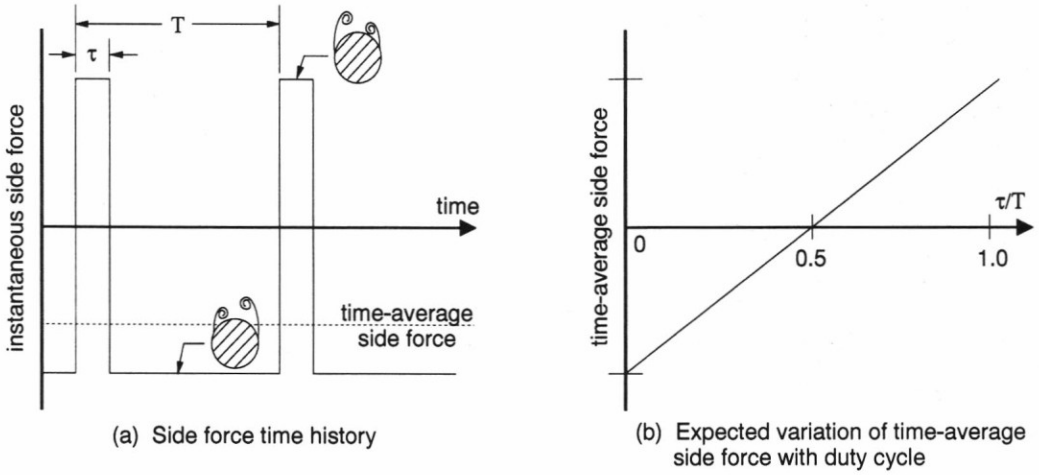

Figure 2 – Concept of dynamic manipulation of forebody vortices.

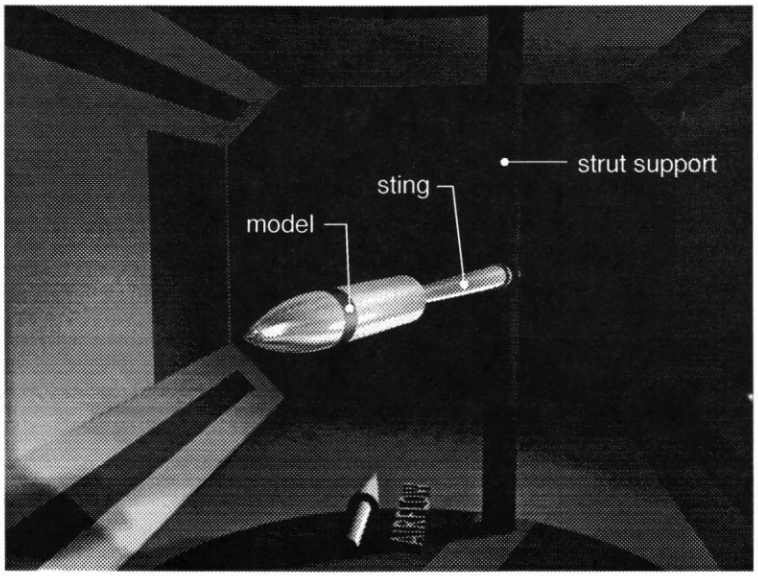

Figure 3 – Wind-tunnel test section with support and model installed.

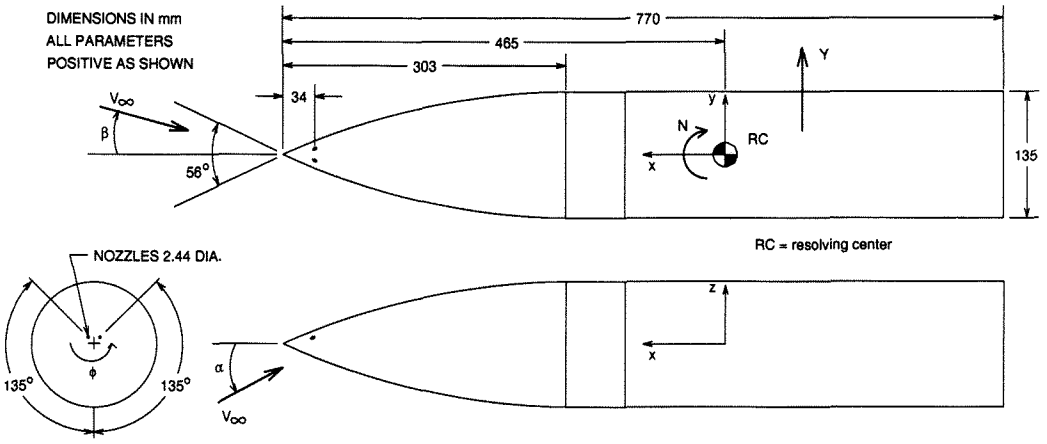

Figure 4 – Wind tunnel model, axis system and sign convention.

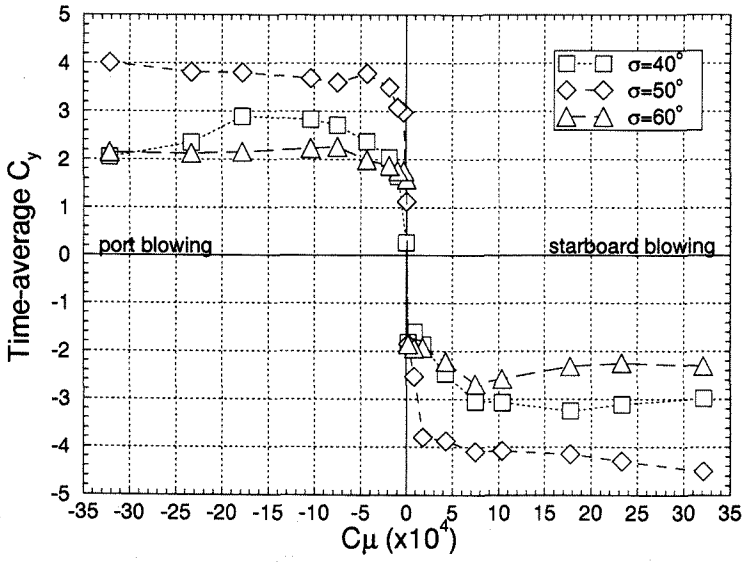

Figure 5 – Time-average side force versus blowing momentum for steady blowing, zero sideslip, $\mathrm{Re}_D = 1.76 \times 10^5$. ($\alpha = \sigma$)

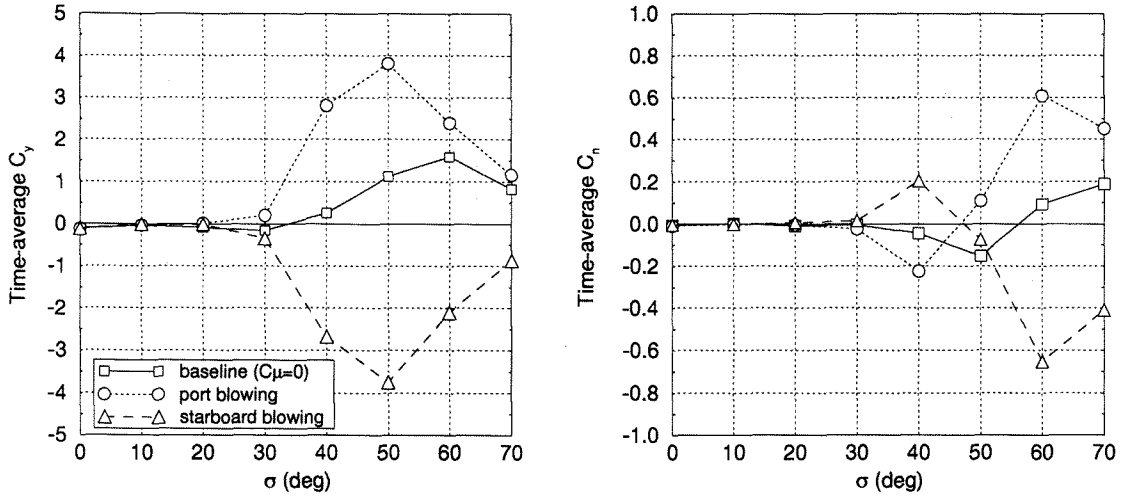

(a) Side force (b) Yawing moment

Figure 6 – Time-average side force and yawing moment versus angle of attack for steady blowing, zero sideslip, $C\mu = 0.00066$, $Re_D = 1.76 \times 10^5$. ($\alpha = \sigma$)

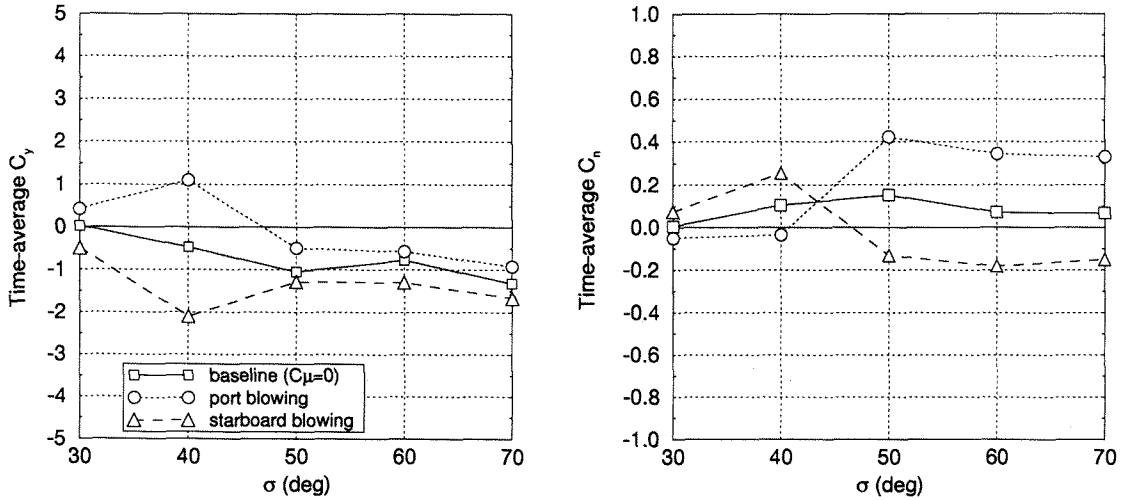

(a) Side force (b) Yawing moment

Figure 7 – Time-average side force and yawing moment versus angle of attack for steady blowing, zero sideslip, $C\mu = 0.00094$, $Re_D = 6.50 \times 10^5$. ($\alpha = \sigma$)

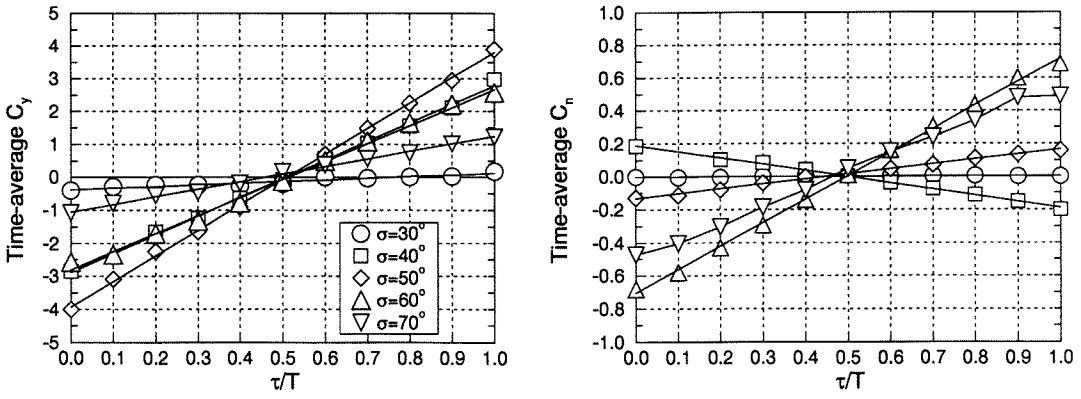

(a) Side force (b) Yawing moment

Figure 8 – Time-average side force and yawing moment for zero sideslip, $\mathrm{Re}_D = 1.76 \times 10^5$, $C\mu = 0.00066$, $\omega^* = 0.16$. $(\alpha = \sigma)$

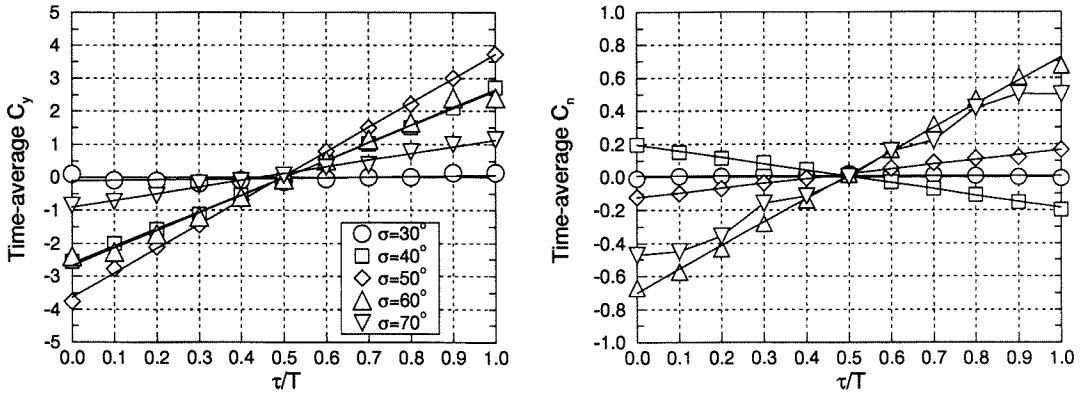

(a) Side force (b) Yawing moment

Figure 9 – Time-average side force and yawing moment for zero sideslip, $\mathrm{Re}_D = 1.76 \times 10^5$, $C\mu = 0.00066$, $\omega^* = 0.32$. $(\alpha = \sigma)$

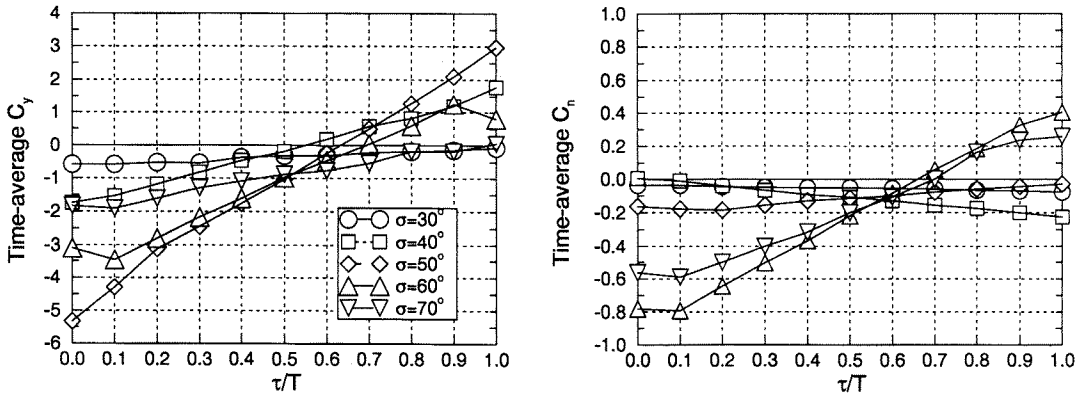

(a) Side force (b) Yawing moment

Figure 10 – Time-average side force and yawing moment for $\phi = 10°$, $\mathrm{Re}_D = 1.76 \times 10^5$, $C\mu = 0.00066$, $\omega^* = 0.32$. $(\cos\alpha = \cos\sigma / \cos\beta,\ \tan\beta = \tan\phi \times \sin\alpha)$

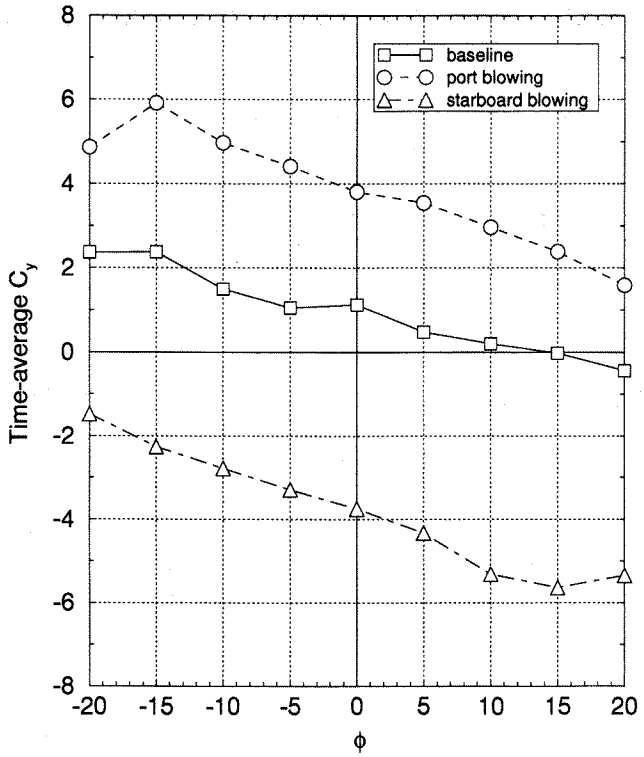

Figure 11 – Effect of roll angle on time-average side force for steady blowing, with $\sigma = 50°$, $C\mu = 0.00066$, $Re_D = 1.76 \times 10^5$. ($\cos\alpha = \cos\sigma / \cos\beta$, $\tan\beta = \tan\phi \times \sin\alpha$)

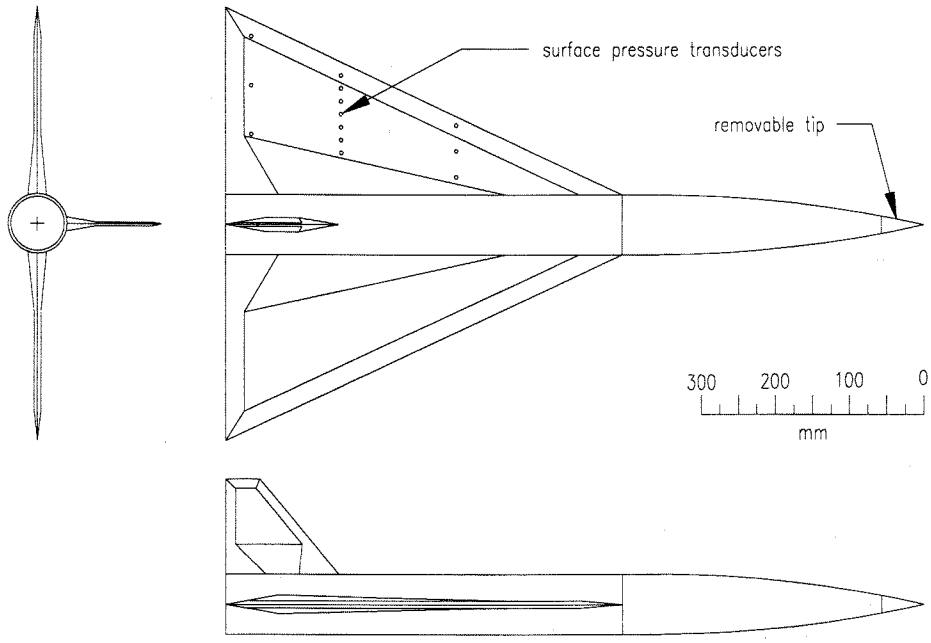

Figure 12 – 65° delta wing model with a long, slender forebody of circular cross-section and a removable tip, to be used in future tests.